Biomaterials 35 (2014) 5472–5481

Contents lists available at ScienceDirect

Biomaterials

journal homepage: www.elsevier.com/locate/biomaterials

Fracture resistance of human cortical bone across multiple length-scales at physiological strain rates

Elizabeth A. Zimmermann [a], Bernd Gludovatz [a], Eric Schaible [b], Björn Busse [a,c], Robert O. Ritchie [a,d,*]

[a] Materials Sciences Division, Lawrence Berkeley National Laboratory, Berkeley, CA, USA
[b] Experimental Systems Group, Lawrence Berkeley National Laboratory, Berkeley, CA, USA
[c] Department of Osteology and Biomechanics, University Medical Center, Hamburg, Germany
[d] Department of Materials Science and Engineering, University of California, Berkeley, CA, USA

ARTICLE INFO

Article history:
Received 23 January 2014
Accepted 22 March 2014
Available online 13 April 2014

Keywords:
Bone
Strain rate
Fracture toughness
Plasticity
X-ray diffraction

ABSTRACT

While most fracture-mechanics investigations on bone have been performed at low strain rates, physiological fractures invariably occur at higher loading rates. Here, at strain rates from 10^{-5} to 10^{-1} s^{-1}, we investigate deformation and fracture in bone at small length-scales using *in situ* small-angle x-ray scattering (SAXS) to study deformation in the mineralized collagen fibrils and at the microstructural level via fracture-mechanics experiments to study toughening mechanisms generating toughness through crack-tip shielding. Our results show diminished bone toughness at increasing strain rates as cracks penetrate through the osteons at higher strain rates instead of deflecting at the cement lines, which is a prime toughening mechanism in bone at low strain rates. The absence of crack deflection mechanisms at higher strain rates is consistent with lower intrinsic bone matrix toughness. In the SAXS experiments, higher fibrillar strains at higher strain rates suggest less inelastic deformation and thus support a lower intrinsic toughness. The increased incidence of fracture induced by high strain rates can be associated with a loss in toughness in the matrix caused by a strain rate induced stiffening of the fibril ductility, *i.e.*, a "locking-up" of the viscous sliding and sacrificial bonding mechanisms, which are the origin of inelastic deformation (and toughness) in bone at small length-scales.

Published by Elsevier Ltd.

1. Introduction

Traumatic injuries, such as falls, often can lead to bone fractures. This fragility is especially significant in the elderly, where broken bones can be associated with a further deterioration in health [1]. As these traumatic injuries invariably result from loading over short time-scales, it is necessary to understand how the structural framework of the human body resists fracture at such physiologically high strain rates.

The fracture resistance of human cortical bone is a direct result of its hierarchically assembled structure of collagen and hydroxyapatite (HA) mineral, which spans multiple length-scales from molecular to near-macroscopic dimensions (Fig. 1) [2,3]. Basically, there are two major contributions to the fracture toughness of bone,[1] namely, intrinsic toughening mechanisms that promote "plasticity", *i.e.*, ductility in the mineralized tissue, and extrinsic toughening mechanisms that act to "shield" a growing crack from the global stresses and strains.[2] The intrinsic toughness represents the inherent fracture resistance of the material and is developed at small (sub-micron) length-scales; here, the fibril can elastically stretch through cooperative deformation between the mineral and collagen [8,9] as well as absorb further deformation through inelastic mechanisms, such as intra/interfibrillar sliding, breaking/reforming of sacrificial bonds, and even through the opening of dilatational bands at the mineral/collagen interface [8,10–12]. The extrinsic toughness of bone, conversely, is a primary function of how the microstructure can inhibit the growth of a crack; essentially, as a

* Corresponding author. Department of Materials Science and Engineering, University of California, Berkeley, CA, USA. Tel.: +1 510 486 5798; fax: +1 510 643 5792.
E-mail address: RORitchie@lbl.gov (R.O. Ritchie).

[1] The fracture toughness can be expressed as the critical value of the stress intensity K for unstable fracture in the presence of a pre-existing crack, *i.e.*, in mode I when $K = Y\sigma_{app}(\pi a)^{1/2} = K_{Ic}$, where σ_{app} is the applied stress, a is the crack length, and Y is a function (of order unity) of crack size and geometry. Alternatively, the toughness can be expressed as a critical value of the strain-energy release rate, G_c, defined as the change in potential energy per unit increase in crack area, or the nonlinear elastic version of G, the J-integral.

[2] Fracture resistance can be considered as a mutual competition between two classes of mechanisms: *intrinsic* mechanisms, which are microstructural damage mechanisms that operate ahead of the crack tip to promote cracking, and *extrinsic* mechanisms, which operate principally in the wake of the crack tip to inhibit cracking by "shielding" the crack from the applied driving force [4–7]. Whereas intrinsic toughening mechanisms, principally plastic deformation, act in general to resist intrinsic microstructural damage and thus are effective in inhibiting both the initiation and growth of cracks, extrinsic toughening mechanisms, *e.g.*, crack bridging, are only effective in inhibiting crack growth [6].

http://dx.doi.org/10.1016/j.biomaterials.2014.03.066
0142-9612/Published by Elsevier Ltd.

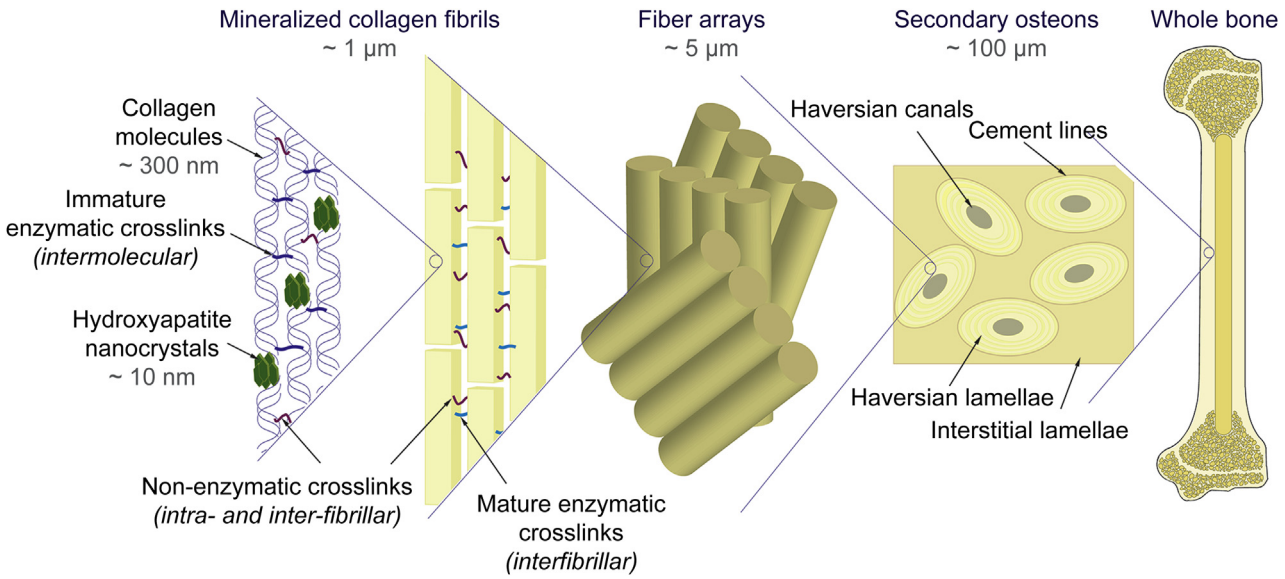

Fig. 1. The structure of human cortical bone spans multiple size-scales, which allows it to develop strength and resistance to fracture. At the smallest length-scales, human cortical bone is composed of an array of collagen molecules embedded with hydroxyapatite (HA) mineral crystals. The collagen and mineral comprises an array of mineralized collagen fibrils with various types of cross-links stabilizing the array and the individual fibrils. At higher length-scales, secondary osteons are the main motif at the microstructural scale. The osteons have a central vascular cavity (the Haversian canal) that is concentrically surrounded by lamellae, which are composed of collagen fibers. At the outer boundary of the osteon is a boundary called the cement line, which has a higher mineralization relative to the surrounding bone matrix. Adapted from Ref. [25].

crack begins to grow, the interaction of the crack path with the microstructure can lead to mechanisms such as crack deflection and bridging, which "shield" the crack tip from the full stress intensity, thereby increasing the bone toughness [6]. Because most cracks are on the micron-scale, these extrinsic toughening mechanisms are most effective when they interact with structural length-scales of comparable dimensions, *i.e.*, ~10s–100s μm, specifically with the osteonal systems through which bone remodels. The osteons consist of circumferential lamellar structures surrounding the Haversian canals (Fig. 1) and with an outer boundary separating the osteon from the interstitial matrix called the cement line, which is thought to have a relatively higher mineralization than the surrounding bone tissue[3] [14,16]. As a large population of the microcracks created in bone form within the interstitial bone (*i.e.*, the bone matrix between the osteons) [17], a growing crack which impinges on the osteonal borders (*i.e.*, the cement lines) is invariably subject to crack deflection and/or twisting,[4] often causing delamination along the cement lines; furthermore, the resulting intact material left between the microcracks can lead to so-called "uncracked ligament" bridges spanning the main crack wake, which further enhance the crack-tip shielding [19,20]. In this manner, through a combination of intrinsic "plasticity" mechanisms at small (sub-micron) length-scales and crack-tip shielding mechanisms at larger length-scales, healthy human cortical bone develops numerous potent mechanisms that can act to resist bone fracture.

Many studies on the strength and toughness properties of human cortical bone have shown succinctly that the complex hierarchical bone-matrix structure at both small and large length-scales is proficient in resisting the initiation and propagation of the major cracks that can cause bone fractures [19,21–26]. However, the reality is that most of these studies have been conducted at low strain rates on the order of 10^{-4} s^{-1} where it is easier to observe and collect data, whereas most physiological bone fractures are generally associated with much higher strain rates. For example, *in vivo* loading rate measurements on bone suggest strain rates of ~0.007–0.013 s^{-1} during walking or running and strain rates as high as ~0.02 s^{-1} during sprinting or downhill running [27–29]; other studies simulating a fall have shown that it takes ~6–10 ms for a falling femur to reach the peak load once it has begun to make contact with the ground [30], with an upper bound for these high strain rates to be ~25 s^{-1} for very high impacts [31]. As these physiologically realistic situations represent strain rates some four or more orders of magnitude higher than those used in most bone fracture experiments in the laboratory, characterizing and understanding the role of loading rate in influencing the multi-scale mechanisms by which bone resists fracture is clearly pertinent.

Previous studies have characterized the strength and toughness of bone at a wide range of strain rates [32–42]. The majority of studies point towards a ductile to brittle transition in bone, where there is a progressive decrease in the amount of post-yield ductility as well as increase in strength and modulus [34–37,40–42]. Notched toughness tests have also been performed at various strain rates and generally show a decrease in toughness at higher strain rates with a corresponding decrease in the accumulation of damage [32,33,38,39].

Consequently, we analyze here the mechanical response of bone over multiple length-scales at physiological strain rates of ~10^{-5}–10^{-1} s^{-1}. Using *in situ* synchrotron small- and wide-angle x-ray scattering/diffraction (SAXS/WAXD) during uniaxial tensile testing and fracture-mechanics-based fracture toughness analyses, we examine the specific roles of plasticity on intrinsic toughness at sub-micron dimensions and the role of crack-tip shielding on extrinsic toughness at the scale of ~1–100s μm to investigate whether the salient mechanisms of toughening in bone are still as effective in resisting bone fractures at physiologically high strain rates.

[3] The composition of the cement lines has been a matter of debate in the literature [13–16]. However, the general consensus is that the cement lines in healthy bone represent regions of high mineralization relative to the surrounding bone matrix or a collagen deficient feature in the bone microstructure [14,16].

[4] The deflection of a crack from a path of maximum tangential stress, essentially the path of maximum strain-energy release rate G, can lead to significant reductions in the crack-driving force experienced locally at the crack tip. Typically, an in-plane crack deflection of ~90° can reduce the stress intensity K at the crack tip by almost a factor of two; if out-of-plane twisting of the crack path occurs, the reduction in the crack-tip K can be even higher [18].

2. Materials and methods

2.1. Materials

The cortical bone from the femur of a 52-year-old male was used for all mechanical testing. The posterior side of the diaphysis/shaft was used in the x-ray scattering experiments, while the samples for toughness testing were taken from the lateral side. Following harvesting, all samples were kept frozen prior to testing, wherein they were machined and then immersed in Hanks' Balanced Salt Solution (HBSS) for at least 12 h.

2.2. Small- and wide-angle x-ray scattering/diffraction

By performing uniaxial tensile tests on small bone samples and subjecting them to real time SAXS and WAXD in the synchrotron light source, we can measure the macroscopic strain in the bone tissue sample, and then partition this strain to determine the individual strains in the fibril (from the SAXS spectra) and HA mineral (from the WAXD spectra) constituents of the bone, based on the procedures initially devised by Gupta et al. [43]. Rectangular samples of human cortical bone in the transverse orientation were sectioned to a thickness of 0.5 mm by using a water-irrigated low-speed saw with a diamond-coated blade. The samples were oriented such that the long axis of the samples was parallel to the long axis of the bone. The samples were then polished with water-irrigated 800 grit silicon carbide paper to final dimensions of roughly 15 mm × 1 mm × 250 μm. Silicon carbide paper was glued to the ends of the samples with cyanoacrylate glue to form frictional surfaces to grip during testing, and then soaked in HBSS for 24 h prior to testing.

The samples were loaded in tension in a custom-made mechanical testing device, with the sample held between two grips, one of which was stationary and the other connected to a displacement stage (model UTMPP1HL, Newport, Irvine, CA) and a 34-kgf load cell (LC703-75, Omega, Stamford, CT). The rig was positioned in beamline 7.3.3 at the Advanced Light Source (ALS) synchrotron radiation facility (Lawrence Berkeley National Laboratory, Berkeley, CA) [44], such that SAXS and WAXD data collection could be recorded simultaneously with mechanical loading. The testing was performed at room temperature with samples hydrated throughout the experiment by means of a hydration cell comprised of a strip of cellophane held to the sample through capillary action with a few drops of HBSS.

The samples were randomly split up into four groups, which were tested at one of four displacement rates. The displacement rates used were 10 mm/s ($N = 12$), 1 mm/s ($N = 3$), 0.1 mm/s ($N = 7$) and 0.001 mm/s ($N = 10$), which produced strain rates on the order of magnitude of 10^{-1}, 10^{-2}, 10^{-3} and 10^{-5} s^{-1}, respectively. As discussed above, a strain rate of 1 s^{-1} corresponds physiologically to a fall whereas strain rates of 10^{-3}–10^{-2} s^{-1} pertain to that experienced when running or walking; for comparison, a strain rate of 10^{-5} s^{-1} was also examined as strain rates near this magnitude have been used in previous laboratory studies.

A high-speed 100k Pilatus detector (Dectris, Baden, Switzerland) was used to collect the SAXS data, while a Pilatus 300K-W detector was used to collect the WAXD data. The SAXS detector was located at the largest allowable distance from the sample (~4100 mm) to detect fine changes in the collagen peak's position, whereas the WAXD detector was placed ~120 mm from the sample at an angle of ~18°.

The highest strain rate tested the limits of data collection from the detectors. To measure deformation in the collagen and mineral at the highest strain rate, a TTL pulse was sent to the SAXS and WAXD detectors to trigger a burst of 300 images. During this period, the sample was exposed to x-rays for 3 ms (*i.e.*, exposure time) and the data were subsequently read out by the detector for 2.5 ms (limit of the detector). Thus, at the fastest strain rate, the SAXS, WAXD, and tissue strain data were acquired every 5.5 ms (*i.e.*, frame interval). For the 10^{-2} s^{-1} strain rate, an exposure time of 30 ms was used with a frame interval of 35 ms. For the strain rate of 10^{-3} s^{-1}, an exposure time of 40 ms was used with a 50-ms frame interval, and for the lowest strain rate of 10^{-5} s^{-1} tests, an exposure time of 500 ms and a frame interval of 10 s were used. The load data were digitized at 2 kHz with a data acquisition card (National Instruments). As radiation damage can affect the mechanical properties of the bone, the total x-ray irradiation dose did not exceed 30 kGy [45].

The strain applied to the bulk sample (*i.e.*, tissue strain) was measured by marking the sample with two sets of horizontal lines. A CCD camera imaged the sample as the loads were applied and the macroscopic tissue strain in the sample was determined from the change in spacing during testing of the horizontal lines on the sample. The tissue strain, ε_t, applied to the samples can then be simply calculated as $\varepsilon_t = \Delta l/l_o$, where $\Delta l = l_i - l_o$ is the change in length between the lines on the sample, and l_i and l_o are, respectively, their instantaneous and initial separations.

2.3. X-ray scattering/diffraction data analysis

The analysis software IGOR Pro (Wavemetrics, Portland, OR) was used in conjunction with the custom macro NIKA [46] to convert the 2-D SAXS data to 1-D. First, the sample-to-detector distance and beam center were calibrated with the 2-D scattering pattern of a silver behenate standard. A mask was created that removed the beamstop, the detector module gaps, and all hot pixels from the 2-D data. The 2-D scattering data were normalized by the x-ray photon counts measured by an ion chamber downstream of the sample. Next, the 2-D data were converted to 1-D data by radially integrating over a 10° sector oriented parallel to the direction of loading. To increase the statistics for the 10^{-1}, 10^{-2}, and 10^{-3} s^{-1} strain rates, the 1-D integrations of the 10° sector above and below the beam center were joined and scattering from the background was subtracted.[5] The location of the first-order collagen peak was found by fitting the 1-D SAXS data with a combination of a linear function and an exponentially modified Gaussian. The strain in the collagen fibrils was measured as the change in position of the first-order collagen peak's center divided by its location at zero load.

The WAXD data used to determine the strain in the mineral were calibrated using an aluminum standard to find the sample-to-detector distance and beam center, as above. The 2-D datasets for the background and bone were normalized by the photon counts and then converted to a 1-D dataset by taking a 4° sector that was aligned with the loading axis. The background was subtracted from each set of bone data and the (0002) peak of the mineral was fit with a Gaussian and linear function. The strain in the mineral was defined as the change in position of the (0002) peak divided by the location at zero load.

2.4. Strength measurements

The fracture surfaces of the samples used in the SAXS testing were imaged with back-scattered electrons in a variable pressure scanning electron microscope (S-4300SE/N SEM, Hitachi America, Brisbane, CA) at a pressure of 35 Pa and an accelerating voltage of 25 kV; the porosity of these fracture surfaces was determined with the image analysis software Fiji [47]. To construct the uniaxial stress–strain curves, the stress during the tensile tests was calculated by normalizing the load values measured during testing by the cross-sectional area of each sample's fracture surface, which excluded porosity and structural voids.

2.5. Fracture toughness testing

15-mm long rectangular bend specimens, with a width of $W \sim 3$ mm and thickness of $B \sim 1.5$ mm, were cut by using a water-irrigated low-speed saw with a diamond-coated blade. The samples were oriented in the transverse orientation, such that the direction of the long axis of the bone, and hence that of the osteons, was parallel to the sample length. The samples were then micro-notched for fracture toughness testing by using a water-irrigated low-speed saw to produce an initial notch. Then, the notch tip was subsequently sharpened by polishing the initial notch with a razor blade irrigated with 1-μm diamond solution to give a crack length of $a \sim 1.5$ mm and a consistent notch root radius of ~3–5 μm. Prior to testing, all of the notched samples were given a final polish in a 0.05 μm diamond suspension and soaked in ambient HBSS for ~24 h. For the highest and lowest displacement rates, four samples were tested per group, while the moderate displacement rate group had five samples.

The samples were tested *in vitro* in three-point bending on a mechanical testing machine (ElectroForce, Bose, Eden Prairie, MN) in Hanks' Balanced Salt Solution (HBSS) at 37 °C and the load–displacement curve was reported. To attain the appropriate strain rates corresponding to the uniaxial tensile tests, the displacement rates for the toughness tests were calculated based on the deformation of an unnotched sample with the same dimensions as the notched sample. Fracture toughness measurements were carried out in general accordance with ASTM Standard E1820 [48] for single-edge notched bend specimens, using nonlinear elastic *J*-integral measurements to incorporate the role of plastic deformation in the determination of the fracture toughness. Specifically, the *J* integral was computed as the sum of elastic, J_{el}, and plastic components, J_{pl}, such that at any point on the load–displacement curve the *J*-integral can be written as follows:

$$J = K^2/E' + J_{pl},$$

where $E' = E$, Young's modulus, in-plane stress and $E/(1 - \upsilon^2)$ in-plane strain, υ is Poisson's ratio (for bone, $\upsilon \sim 0.3$), and K is the linear-elastic stress intensity calculated as follows:

$$K = \frac{PS}{BW^{3/2}} f(a/W)$$

[5] To determine the contribution of scattering from the background, SAXS and WAXD data were also acquired with no sample present; the background included scattering from the air, hydration cell as well as HBSS and was taken at the corresponding exposure time. The background data were normalized by the x-ray photon counts and radially integrated over a 10° sector parallel to the loading direction.

where P is the applied load, S is the major (three-point) loading span, and $f(a/W)$ is a geometry dependent function of the crack length to width ratio provided in ASTM Standard E1820 [48]. The plastic component of J is calculated from the following equation:

$$J_{pl} = \frac{\eta A_{pl}}{Bb},$$

where $\eta = 1.9$, A_{pl} is the plastic area underneath the load–displacement curve, and b is the uncracked ligament width (*i.e.*, $b = W - a$). Using this formulation, the value of J can be determined at any point along the load–displacement curve. For this analysis, the point of fracture on the load–displacement curve was used to calculate the critical mode I value, J_{Ic}.

Fracture toughness values expressed in terms of the stress intensity were then computed using the standard J–K equivalence (mode I) relationship $K_{JIc} = (E' J_{Ic})^{1/2}$, where J_{Ic} is the fracture toughness measured in terms of J and E' is the plane-strain elastic modulus. Values of E for the cortical bone have previously been determined using nano-indentation in young and aged human femoral samples [49]. The results showed a true elastic modulus of approximately 15.70 ± 3.5 GPa for young bone and 15.85 ± 3.3 GPa for aged bone.

For all fracture toughness tests conducted, conditions for J-dominance, as specified by ASTM Standard E1820 [48], were met at the high and moderate strain rates, *i.e.*, $b, B >> 10\,(J/\sigma_y)$, where σ_y is the flow stress. This latter criterion ensures that the critical J_{Ic} (and calculated K_{JIc}) values represent valid fracture toughness values. However, a single value toughness test is not optimal for low strain rate conditions, where the toughness increases with crack growth and is best captured through a crack-growth resistance curve, or R-curve. In terms of ASTM Standard 1820 [48], all single-value toughness measurements at low strain rates were within the maximum J-integral capacity of the samples (equivalent to a stress intensity of 16.4 MPa.m$^{1/2}$).

Fracture surfaces and crack–path profiles were imaged in the variable pressure scanning electron microscope, which was operated at 25 kV accelerating voltage in the secondary electron mode at high vacuum and in back-scattered electron mode at a pressure of 35 Pa.

2.6. Statistics

To test for differences between the strain rates in the fracture-mechanics data, a univariate ANOVA with post-hoc tests was performed under Bonferroni correction for multiple comparisons. p-Values less than 0.05 were considered significant.

3. Results

3.1. Fracture toughness

Fracture toughness tests were performed at three different strain rates. The corresponding critical values of the fracture toughness of the human bone at each strain rate are shown in Fig. 2, where significant overall differences were found between the study groups ($p = 0.009$). Additionally, *post hoc* tests indicate a significant decrease in toughness by 33% from the lowest to highest strain rates ($p = 0.008$). A similar trend has been observed by Kulin et al. [38,39] for equine bone and Adharapurapu et al. [32] for bovine bone (Fig. 2).

The decrease in toughness values at the higher loading rates is consistent with observations of the crack paths and their effect on the magnitude of the extrinsic toughening mechanisms. Observations of the crack path following testing (Fig. 3) indicate that the extent of crack deflection, particularly as the cracks encountered the osteons, was progressively diminished at increasing strain rates. At low strain rates, cracks tend to deflect macroscopically with a corresponding torturous crack path (Fig. 3a); the deflected and twisted crack path can be associated with the crack following the cement lines, as observed at higher magnifications by the incidence of either osteons protruding from the surface or osteons surrounded by a circular shell rising above them (Fig. 3b). In contrast to the complex path of the crack around osteons at low strain rates, the incidence and extent of such deflection was far less apparent at the highest strain rates, where relatively smoother fracture surfaces are observed (Fig. 3c). This behavior is also manifested in the nature and morphology of the fracture surfaces at higher magnifications (Fig. 3d), where the crack path progresses transversely across the face of the osteons with little evidence of crack deflection at the cement lines. Clearly, fractures occur by more tortuous paths at low strain rates as cracks tend to follow the

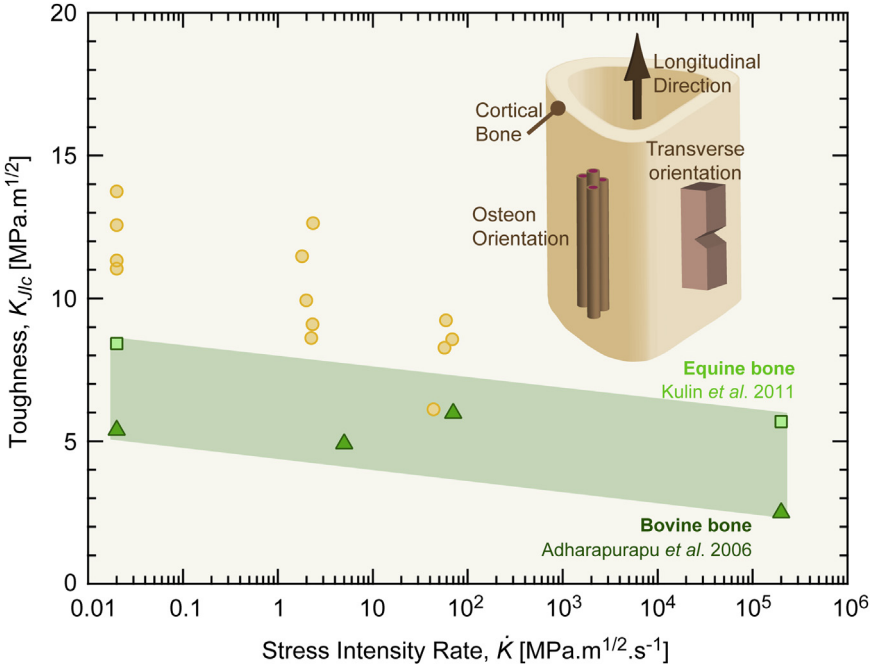

Fig. 2. The mechanical properties of human cortical bone were tested at three stress-intensity rates ($\dot{K}$) corresponding to physiological strain rates: the highest strain rate approaching that of a fall ($\sim 1\ s^{-1}$), the moderate strain rate to running ($\sim 10^{-2}\ s^{-1}$), and the lowest strain rate typical of most mechanical tests on bone in the literature ($\sim 10^{-4}\ s^{-1}$). The corresponding fracture toughness, K_{JIc}, is plotted as a function of the stress-intensity rate. Bone clearly displays a significantly higher toughness ($\sim$33% higher) at the lower strain rate ($p = 0.008$) consistent with the observation that the bone–matrix structure is able to absorb more energy during slower deformation. The data presented here for human cortical bone are consistent with prior studies on bovine [32] and equine [39] bone.

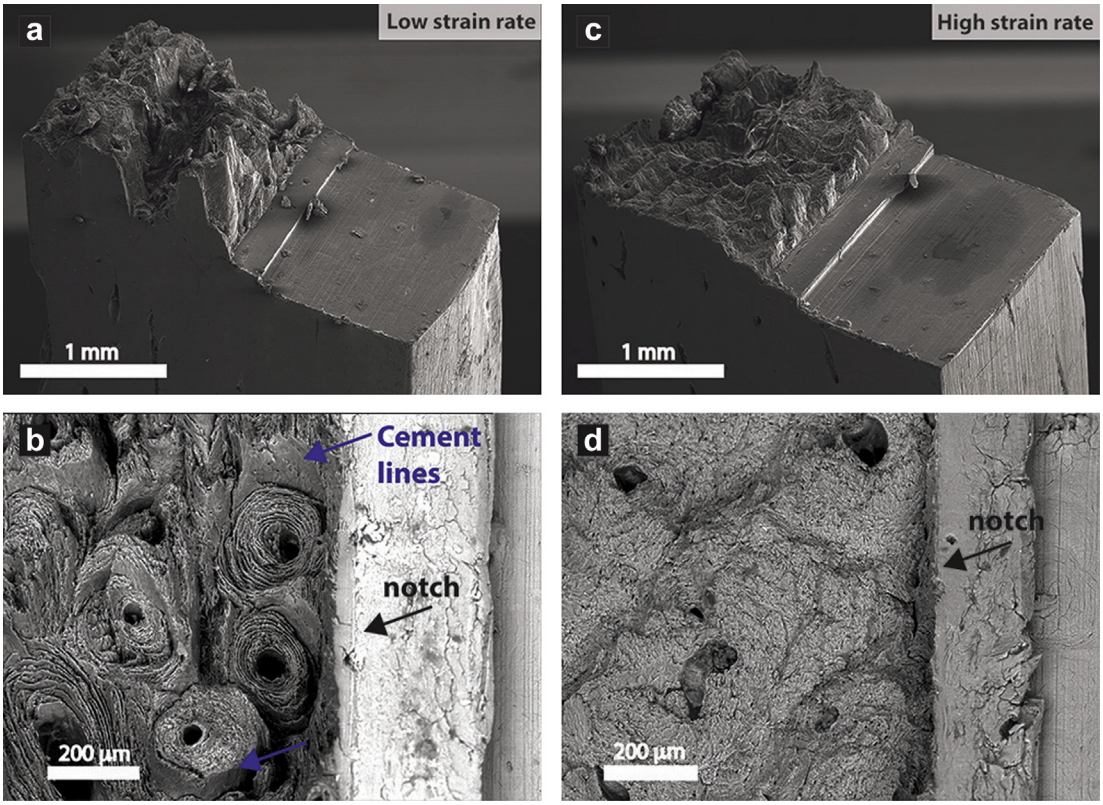

Fig. 3. The fracture surfaces of the toughness samples were observed in the scanning electron microscope following fracture toughness measurements. For the low loading rate tests corresponding to lower strain rates, (a) cracks follow an expected deflected path through the microstructure, consistent with the rough fracture surfaces which indicate a tortuous fracture path with numerous twists and deflections. (b) A closer examination at high magnification shows whole osteons either protruding from the surface or containing a circular shell rising above them suggesting that the crack deflected at, and then followed, the cement lines as it advanced through the bone–matrix structure. Such highly twisted and deflected crack paths provide a major contribution to the extrinsic toughness of bone. For the toughness tests at the highest loading rate corresponding to the highest strain rate, (c) cracks in the bone followed a distinctively straighter path, with a smoother and less tortuous fracture profile (*i.e.*, less crack deflection and twist). (d) The corresponding high-resolution SEM imaging revealed that the crack grew across the osteons and did not take a circuitous route around the cement lines. Thus, as the strain rate increases, the toughening mechanism of crack deflection along the brittle cement lines appears to be less effective. The crack is growing from right to left in all images.

cement lines that act as preferential locations for microcracking due to their higher mineralization in comparison to the surrounding bone tissue, thereby promoting toughening via crack deflection and twist; this critical extrinsic toughening mechanism, however, is significantly curtailed at the higher strain rates.

3.2. Strength

The strength of bone samples from a single donor was measured in uniaxial tension during the SAXS/WAXD tests in the x-ray synchrotron. The resulting stress–strain curves are shown in Fig. 4a for the four strain rates tested ranging from 10^{-1} to 10^{-5} s^{-1}. From these results, it is apparent that bone strength actually increases at higher strain rates whereas the ductility of the bone, as measured by the post-yield plastic deformation, is diminished,[6] which is in agreement with previous mechanical tests [31,35,50].

[6] The observation that the bone ductility is lower as the strain rate is increased is somewhat difficult to assess because the current SAXS/WAXD setup was not optimized to acquire a precise value of maximum strain. Specifically, we collect data points at fixed intervals to avoid over-irradiating the bone at slow strain rates and to allow data read-out at high strain rates. If the sample breaks in between data collection points, then precise data for the maximum strain will not be collected. This error, however, is relatively small, and we believe that the results still clearly show that the extent of plasticity, as measured by the post-yield strain, is definitely reduced with progressively increasing strain rates.

3.3. Small- and wide-angle x-ray scattering/diffraction

Results from the *in situ* SAXS analysis of the uniaxial tensile tests at the four strain rates, shown in Fig. 4b, indicate the individual strain in the mineralized collagen fibril as a function of macroscopic tissue strain in the bone sample. Despite the difficulty in obtaining precise data at the highest strain rate of 10^{-1} s^{-1} due to the short exposure times (see Appendix Fig. A1), there is a trend towards a higher proportion of strain being transferred to the fibril with increasing strain rate, implying a distinct strain-rate dependent change in the deformation mechanisms in the bone at small length-scales. A rate-dependency in the mineral strain was not observed.

4. Discussion

The question posed here is whether the strength and toughening mechanisms found at lower strain rates are as effective in inhibiting bone fractures at the high strain rates associated with physiological activity and fracture incidents. To address this, we have investigated the toughness of bone at both small length-scales, using SAXS/WAXD experiments to examine its strength and plasticity, and at larger length-scales, using a fracture-mechanics characterization of the toughness and corresponding crack trajectories, at strain rates between 10^{-1} and 10^{-5} s^{-1}.

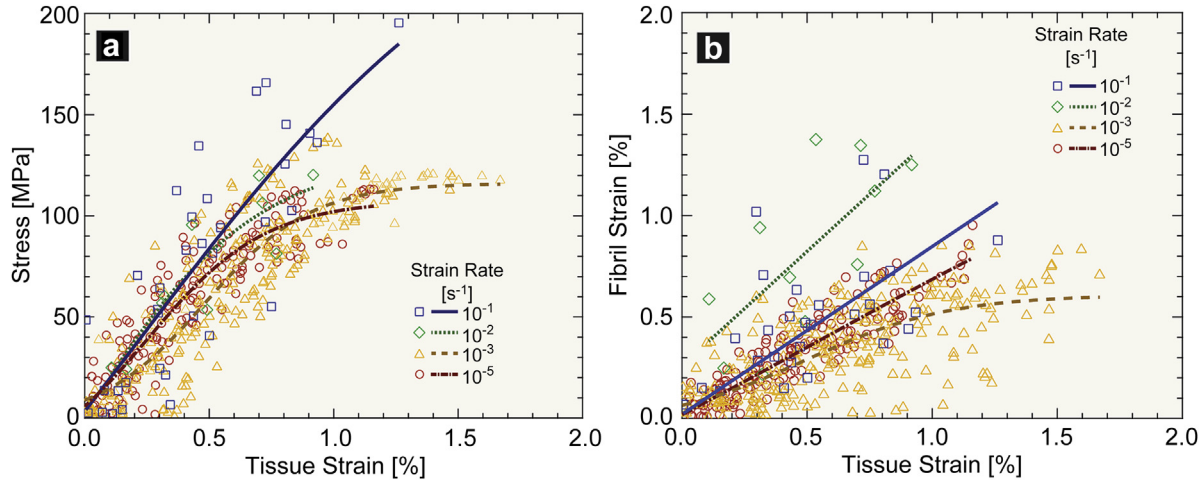

Fig. 4. Samples of human cortical bone from a single donor were mechanically tested in uniaxial tension at the Advanced Light Source beamline 7.3.3, while simultaneously exposing the samples to x-rays and collecting the resulting (a) stress–strain curves as well as the (b) small-angle x-ray scattering (SAXS) data. The mechanical tests were performed at four different strain rates, which made use of the beamline's fast image acquisition capabilities. (a) The stress–strain curves show that as the strain rate increases, the bone loses plasticity as the curves are straighter at higher strain rates. (b) As the bone samples are exposed to x-rays during tension testing, the *d*-period of the fibrils causes diffracted arcs on the detector. As the bone is mechanically tested in tension, the fibrils stretch within the bone causing increases in their *d*-period, which are reflected in the position of the diffracted arcs on the detector. Thus, the strain in the mineralized collagen fibril can be measured by the shift in the arc position in the SAXS data. Here, the fibril strain tends to increase at higher strain rates resulting in fibrils with a higher strain for a given tissue strain. As the viscosity of bone has large contributions from its hierarchical structure, we believe the fibril is subjected to a higher strain at high strain rates due to a "locking-up" of the inelastic toughening mechanisms that are the source of plasticity in bone. Note that the results for the highest strain rate required very fast exposure and data collection times to collect SAXS data during the rapid mechanical test, which hampered the precision with which we could collect the data, see Appendix.

4.1. Extrinsic toughness

From the results of the fracture toughness experiments, the resistance of cortical bone to fracture clearly diminishes by roughly 33% at higher strain rates (Fig. 2) indicating a change in the bone's extrinsic resistance to fracture. At the microstructural scale ($\sim$10–100 μm), we find the lower toughness to be associated with a distinct change in crack path in relation to the bone-matrix structure, which has a definitive effect on the generation of extrinsic toughness in the bone. Images of the fracture surfaces after micro-notched three-point bending tests indicate that at lower strain rates, the crack takes a tortuous path through the bone-matrix structure and deflects at the cement-line boundaries of the osteons, which have a higher mineralization in comparison to the surrounding bone tissue (Fig. 3a,b). This crack deflection (and/or crack twist) increases the toughness as a function of crack extension because of the induced change in the mode-mixity at the crack tip, which reduces the overall stress intensity. In contrast, at higher strain rates, crack deflection at the cement line is effectively absent such that the crack takes a straighter crack path that penetrates across the face of the osteon (Fig. 3c,d). The absence of the crack deflection mechanism, which significantly decreases the extrinsic contributions to the bone toughness, can be readily coupled with the reduced intrinsic toughness of bone resulting from diminished plasticity at higher strain rates, as discussed below.

To provide a relatively simple explanation why higher strain rates would cause a growing crack in bone to be more likely to cut through the osteons rather than deflect at the cement lines, we can use the theoretical framework of He and Hutchinson [51] for a linear-elastic crack impinging on the interface between two dissimilar materials, following the approach used to examine the effect of the dentin-enamel interface in teeth [52] and the osteonal interface in bone [53]. The conditions for a crack penetrating, as opposed to arresting at, or delaminating along, an interface between two dissimilar materials, termed 1 and 2, depend on (i) the elastic (Young's) modulus E mismatch of materials across the interface, which is captured with the first Dundurs' parameter $\alpha = (E_1 - E_2)/(E_1 + E_2)$, and (ii) the ratio of the toughness of the interface, expressed in terms of the strain-energy release rate G_{int}, to the toughness of the material into which the crack will propagate, G_2, as shown for a normally incident crack in Fig. 5. To apply this formulation to bone (Fig. 5), we first let the crack start in the interstitial bone, with modulus E_1, and let the crack impinge on the cement line interface with toughness G_{int} that surrounds an osteon with modulus E_2 and toughness G_{osteon}. If the values of the elastic mismatch and G_{int}/G_{osteon} are above the line in Fig. 5, the crack will penetrate into the osteon, whereas if the values are below the line, the crack will be deflected along the interface. For the analysis presented here, we assume that the value of α and the toughness of the highly mineralized cement line interface remain essentially insensitive to strain rate.[7]

Applying this approach, we know that because crack deflection occurs at the osteonal interfaces at low strain rates, the elastic mismatch and toughness ratio must result in conditions to be beneath the line in Fig. 5, where a crack impinging on an interface between dissimilar materials causes crack deflection. As the strain rate increases, our fracture experiments indicate that we must cross the line in Fig. 5 towards the region where conditions cause the crack to penetrate the interface. As stated above, if the elastic mismatch and toughness of the interface are unlikely to be affected by strain rate, then crack penetration through the osteons at high strain rates would only be viable if the toughness of the bone matrix decreased (such that conditions fall above the curve). The

[7] Although the modulus of bone has been shown to increase with high strain rate [31,35,50], the relative change in modulus between osteonal and interstitial bone with strain rate is largely unknown; however, the moduli for each region will most likely change proportionally and leave a similar elastic mismatch as at low strain rates. Therefore, we believe it is a reasonable assumption that the elastic mismatch will not be affected significantly by strain rate.

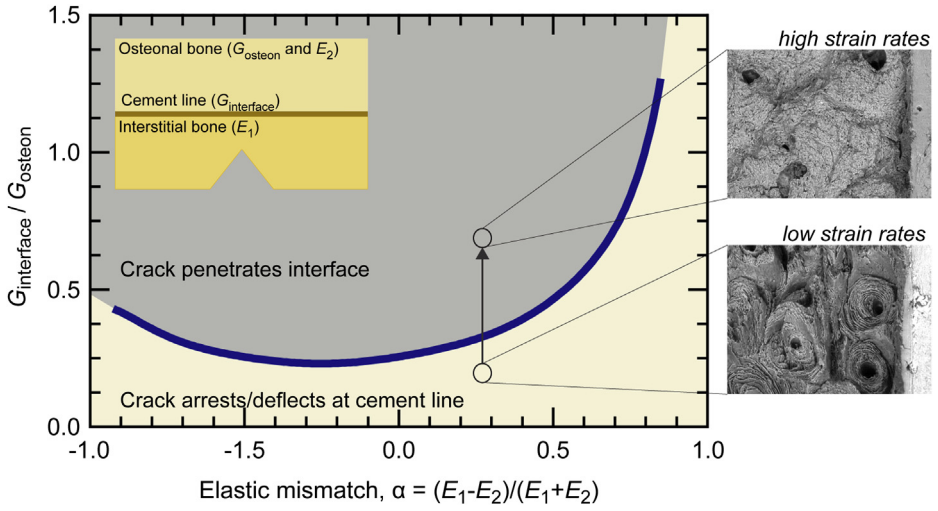

Fig. 5. To theoretically determine whether a crack at an interface between two dissimilar materials will deflect at the interface or penetrate through the interface, the He and Hutchinson [51] framework is applied, shown here for a normally incident crack. Based on the ratio of the interfacial toughness and the toughness of the osteonal bone, both expressed in terms of the strain-energy release rate G, as well as Dundurs' parameter, α (in this case, the elastic mismatch between interstitial and osteonal bone), we can determine whether the point lies above or below the critical condition. Based on the assumption that the toughness of the cement line remains constant and that the relative elastic parameters change relatively with strain rate, conditions would change from the crack deflecting at the interstitial bone/osteon (cement line) interface at low strain rates to one at high strain rates where an incident crack would penetrate the interface, if the toughness of the osteon decreases at such high rates.

implication of this result is that when loading is applied to bone at a higher rate, the bone-matrix structure ahead of a growing crack has the effect of appearing to be less ductile, *i.e.*, displaying less plasticity or toughness, and as a result, the cement lines are no longer a source of extrinsic toughening through the generation of deflected crack trajectories.[8]

4.2. Intrinsic toughness

The intrinsic toughness of the bone describes its inherent resistance to fracture, which primarily originates through plasticity mechanisms at small length-scales. As the fracture toughness results suggest that the bone matrix toughness diminishes at higher strain rates, we used SAXS/WAXD to study the intrinsic toughening mechanisms at the fibrillar scale.

Previous experimental and molecular dynamics studies on unmineralized and mineralized collagen fibrils indicate that during elastic (recoverable) straining, fibrillar deformation occurs through stretching of the fibrils [8,9,11,25]. At the onset of inelastic deformation, slippage and/or sliding mechanisms between the collagen and mineral components as well as between fibrils have been proposed and may include the breaking/reforming of sacrificial bonds and/or the formation of dilatational bands [10–12,25,56]. These deformation mechanisms allow the bone to absorb deformation energy during inelastic (post-yield) straining.

Through small-angle x-ray scattering, we investigated fibrillar deformation at low and high strain rates. At slower strain rates, we found that the fibrillar strain linearly increases with tissue strain (*i.e.*, applied strain) in the elastic region implying stretching of the fibril (Fig. 4b). As the applied strain increases, a plateau is reached. At this point, essentially the maximum strain of the fibril has been reached and further deformation is proposed to occur through inelastic mechanisms, such as sliding between fibrils, or possibly microcracking at higher length-scales. This inelastic deformation allows the bone to develop intrinsic toughness because the higher length-scales can deform rather than induce complete fracture of the fibrils [25].

At higher strain rates, the fibril strain *vs.* tissue strain has a higher slope (Fig. 4b), especially for the two highest strain rates. The higher slope at higher strain rates implies that for a given tissue strain, more strain or deformation occurs within the fibril. The fact that more strain occurs within the fibril implies that mechanisms responsible for bone's inelasticity (*i.e.*, fibrillar sliding, sacrificial debonding, *etc.*) are constrained because deformation is not dissipated through these inelastic mechanisms but directly results in fibril stretching. We believe that this behavior is related to the viscosity or time-dependent nature of the deformation of the whole mineralized collagen fibril structure.

To study this in further detail, we need to focus on the origins of inelastic deformation within the bone. A common assertion in the literature has been that bone develops its toughness from its collagen constituents, which naturally have viscoelastic material behavior in comparison to the whole bone or the mineral. However, recent experimental and computational studies have found that the whole fibril (in this case, unmineralized) is more viscous than a single collagen molecule [9,57]. This plays on the idea that while strength comes from stretching of the fibril (*i.e.*, composite of collagen and mineral), toughness comes from the hierarchical architecture, which allows damage tolerance [58]. Thus, the viscous or inelastic nature of bone may not originate completely from the collagen constituent but from the multi length-scale architecture, in this case of the fibril. Indeed, the arrangement of collagen and mineral within the fibril as well as the relative assembly of fibrils allows sliding within and between fibrils, sacrificial length-scales, and the opening of dilatational bands or microcracks, which all allow bone to deform inelastically.

With respect to the SAXS results, we see more strain in the fibril because the viscous mechanisms essentially "lock-up" at the higher

[8] Comparable effects can occur in bone with aging, irradiation damage and disease where abnormal mineralization, and/or cross-linking profiles within the matrix can reduce the relative inhomogeneity between the bone matrix and the cement lines, again contributing to less deflected crack paths [25,45,54,55].

strain rates, *i.e.*, strain-rate stiffening akin to the behavior of a dashpot at high rates of deformation. However, instead of restricting stretching (as a higher cross-link profile would do), the loss in viscosity allows the fibril to stretch further. Thus, at slower strain rates, the fibrils have a certain amount of plasticity and energy absorption through sliding mechanisms within and between fibrils, while at higher strain rates, the sliding mechanisms lock-up causing the fibrils themselves to stretch further, accounting for less overall plasticity, but higher strength, in the macroscopic properties.

Studies at low strain rates provide a pathway towards understanding the complexities of deformation in human bone and the mechanisms at multiple size-scales that resist bone fracture. However, studies such as this that simulate physiological conditions reinforce the necessity to incorporate the physiological conditions of environment and disease in order to make progress towards decreasing the incidence of bone fracture.

Finally, the shortcomings of this study should be noted in that testing at the physiological strain rates required us to test the limits of the experimental equipment and the flux limits of a third-generation synchrotron. Specifically at high strain rates, short exposure times and fast data collection times were required to make multiple measurements along the stress–strain curve for each sample. Both of these factors reduce the number of scattering events captured on the SAXS detector, which in turn reduces the precision with which we can measure the fibrillar and mineral strains at the highest strain rate. The precision of the strain measurement is given in Appendix Fig. A1 and should be regarded as a limitation of this study. An additional limitation is the use of a single human donor for the experiments. While testing the effects of strain rate on a single donor eliminates the confounding factors of inter-individual variability, only using a single donor does pose a limitation to broadly applying the results to a larger population.

5. Summary and conclusions

Human cortical bone is a complex hierarchical composite that allows deformation at numerous length-scales throughout its structure. At low strain rates, bone resists fracture through the stretching of the mineralized fibrils followed by the generation of plasticity through inelastic mechanisms, such as intra-/interfibrillar sliding, sacrificial bonding, and dilatational band formation. Additionally, at the micron length-scale, the microstructure resists crack growth through the mechanisms of crack deflection along cement lines and uncracked-ligament bridging that both increase the bone's extrinsic toughness.

The results of this study indicate that these toughening mechanisms may change as bone is loaded at higher strain rates. First, at large length-scales, the bone has a lower toughness associated with straighter crack paths across osteons, in comparison to the tortuous crack path taken along the cement lines at low strain rates. The loss in the extrinsic crack deflection mechanism implies that the toughness of the bone matrix must be lower at higher strain rates. SAXS experiments support a lower matrix toughness by indicating that a greater proportion of the applied strain is transferred to the fibrils at high strain rates, which may be due to the "locking-up" of the viscous mechanisms promoting inelastic or intrinsic toughness.

Specifically, we conclude that:

1. Strength tests reveal a progressive loss in plasticity as strain rate increases, which indicates that structural mechanisms promoting inelastic deformation change with strain rate.
2. As the strain rate (or stress-intensity rate) increases (by some four orders of magnitude), the fracture toughness decreases by some 33%. Cracks propagate across the osteonal matrix taking a straighter path than at lower strain rates, where the toughness increases as cracks deflect and follow the cement lines. The absence of crack deflection at the osteonal interfaces represents a significant loss in extrinsic toughness of the bone.
3. The fact that the cracks do not deflect at the osteonal interfaces at higher strain rates can be qualitatively explained through a He and Hutchinson analysis. Essentially, if the bone matrix toughness (*i.e.*, the energy absorption capability) decreases in relation to the toughness of the cement line, then the crack will penetrate the cement line instead of arresting or deflecting along it.
4. SAXS/WAXD allows us to investigate deformation at the fibrillar and mineral length-scales. As the strain rate increases, the fibrils carry a higher proportion of strain. Indeed, the viscous nature of the deformation mechanisms in bone is deemed to originate not only from the collagen molecules but also from the hierarchical structure of the collagen fibrils and fibers. Inelastic deformation within the fibrils essentially "locks-up" at increasing strain rate; consequently the fibrils are subjected to an increasing stretch with less contributions from the viscous toughening mechanisms, which may include intra- and interfibrillar sliding, dilatational band formation, microcracking and breaking/reforming of sacrificial bonds.

Acknowledgments

This work was supported by the National Institute of Health (NIH/NIDCR) under grant no. 5R01 DE015633 to the Lawrence Berkeley National Laboratory (LBNL). BB was supported by the Emmy Noether program of the German Research Foundation (DFG) under grant number BU 2562/2-1. We acknowledge the use of the x-ray synchrotron beamline 7.3.3 (SAXS/WAXD) at the Advanced Light Source (ALS) at LBNL, which is funded by the Office of Science of the U.S. Department of Energy under contract no. DE-AC02-05CH11231. The authors wish to thank Dr. Tony Tomsia at LBNL for his support.

Appendix. Interpretation of SAXS data at high strain rates

Small-angle x-ray scattering during mechanical tension tests is a commonly used technique to investigate the strain at the fibril length-scale in relation to the deformation applied at the whole bone level [25,43,59]. However, even at low strain rates (such as 10^{-5} to 10^{-3} s^{-1}), small variations in data are to be expected. These variations can be caused by the heterogeneity of the bone structure, associated with the inherent variability in composition and structure at the local scale. The consequent scatter in measured mechanical properties of the collagen fibrils is not uncommon and has also been reported with other techniques, such as atomic force microscopy [60,61].

The SAXS technique does pose further limitations at fast strain rates. The experimental limitations of the equipment specifically apply to the fastest strain rate of 10^{-1} s^{-1} where the fast data collection times reduce the number of scattering events that can be captured (see Fig. A1a,b). The reduced number of scattering events can then lower the precision of the fibril *d*-spacing measurement. Such fibril strain measurements at fast strain rates are thus affected by the precision of data measurement and by local variations in structure.

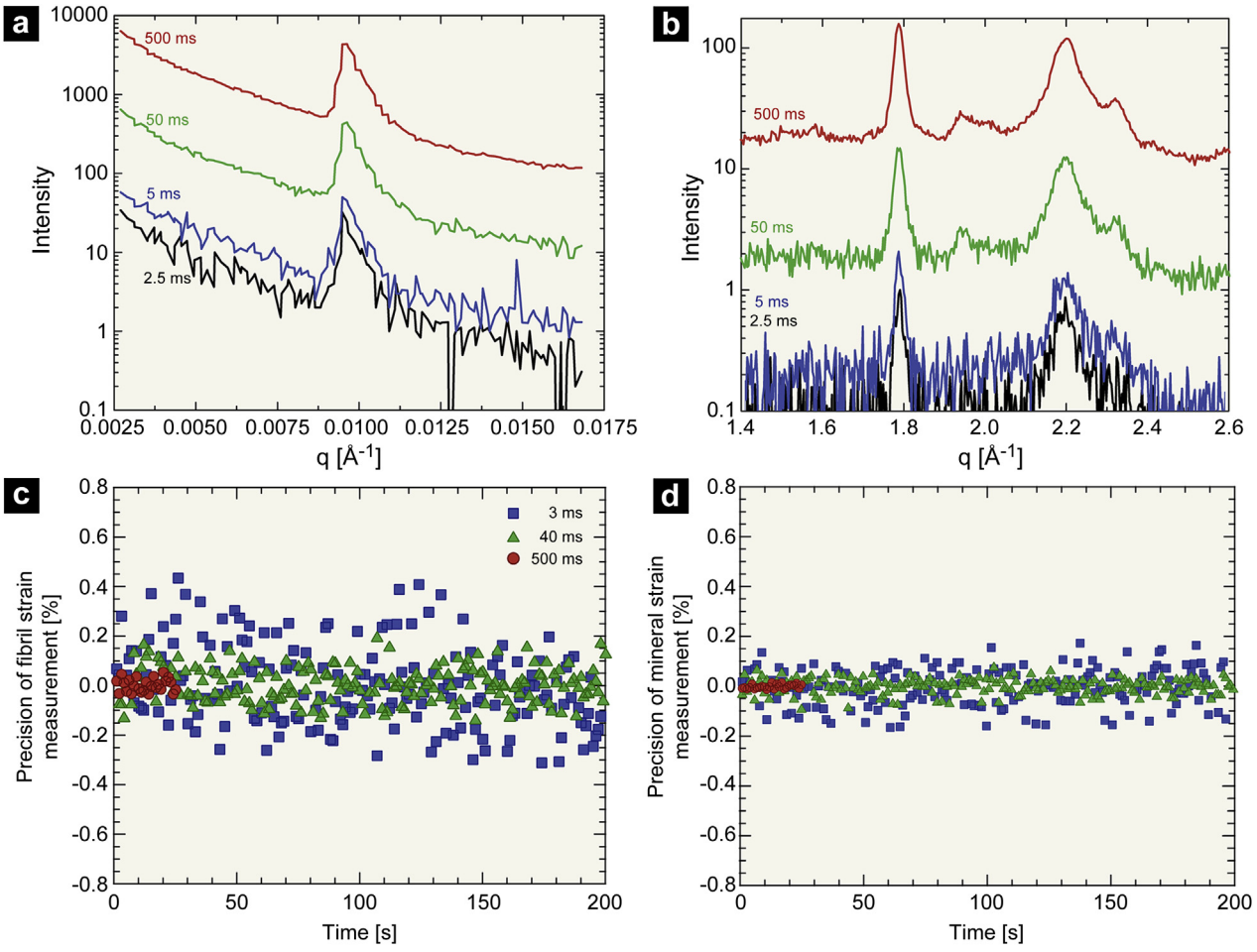

Fig. A1. As the strain rate is increased, faster data collection rates are required to perform the SAXS and WAXD measurements within the time frame of the mechanical test. The faster data collection also requires that the samples be exposed to x-rays for a shorter time. Lowering the exposure time from 500 ms to 2.5 ms results in a severe loss in the intensity of the SAXS (a) and WAXD (b) data because less x-rays are interacting with the sample. Thus, the precision with which the peak center can be determined deteriorates. This is certainly clear in panels (c) and (d) which show the precision of the fibril and mineral strains, respectively, in undeformed samples at the three exposure times used in the 10^{-5} (500 ms), 10^{-3} (40 ms) and 10^{-1} (3 ms) strain rates.

References

[1] Cummings SR, Melton LJ. Epidemiology and outcomes of osteoporotic fractures. Lancet 2002;359:1761–7.
[2] Weiner S, Wagner HD. The material bone: structure mechanical function relations. Annu Rev Mater Sci 1998;28:271–98.
[3] Zimmermann EA, Barth HD, Ritchie RO. On the multiscale origins of fracture resistance in human bone and its biological degradation. JOM 2012;64:486–93.
[4] Evans AG. Perspective on the development of high-toughness ceramics. J Am Ceram Soc 1990;73:187–206.
[5] Launey ME, Ritchie RO. On the fracture toughness of advanced materials. Adv Mater 2009;21:2103–10.
[6] Ritchie RO. Mechanisms of fatigue crack-propagation in metals, ceramics and composites – role of crack tip shielding. Mater Sci Eng A 1988;103:15–28.
[7] Ritchie RO. Mechanisms of fatigue-crack propagation in ductile and brittle solids. Int J Fract 1999;100:55–83.
[8] Buehler MJ. Molecular nanomechanics of nascent bone: fibrillar toughening by mineralization. Nanotechnology 2007;18:295102.
[9] Silver FH, Christiansen DL, Snowhill PB, Chen Y. Transition from viscous to elastic-based dependency of mechanical properties of self-assembled type I collagen fibers. J Appl Polym Sci 2001;79:134–42.
[10] Fantner GE, Hassenkam T, Kindt JH, Weaver JC, Birkedal H, Pechenik L, et al. Sacrificial bonds and hidden length dissipate energy as mineralized fibrils separate during bone fracture. Nat Mater 2005;4:612–6.
[11] Gupta HS, Wagermaier W, Zickler GA, Aroush DRB, Funari SS, Roschger P, et al. Nanoscale deformation mechanisms in bone. Nano Lett 2005;5:2108–11.
[12] Poundarik A, Diab T, Sroga GE, Ural A, Boskey AL, Gundberg CM, et al. Dilational band formation in bone. Proc Natl Acad Sci USA 2012;109:19178–83.
[13] Burr DB, Schaffler MB, Frederickson RG. Composition of the cement line and its possible mechanical role as a local interface in human compact bone. J Biomech 1988;21:939–45.
[14] Busse B, Hahn M, Soltau M, Zustin J, Püschel K, Duda GN, et al. Increased calcium content and inhomogeneity of mineralization render bone toughness in osteoporosis: mineralization, morphology and biomechanics of human single trabeculae. Bone 2009;45:1034–43.
[15] Schaffler MB, Burr DB, Frederickson RG. Morphology of the osteonal cement line in human bone. Anat Rec 1987;217:223–8.
[16] Skedros J, Holmes J, Vajda E, Bloebaum R. Cement lines of secondary osteons in human bone are not mineral-deficient: new data in a historical perspective. Anat Rec A 2005;286A:781–803.
[17] Busse B, Djonic D, Milovanovic P, Hahn M, Püschel K, Ritchie RO, et al. Decrease in the osteocyte lacunar density accompanied by hypermineralized lacunar occlusion reveals failure and delay of remodeling in aged human bone. Aging Cell 2010;9:1065–75.
[18] Faber KT, Evans AG. Crack deflection processes. I. Theory. Acta Metall 1983;31:565–76.
[19] Koester KJ, Ager JW, Ritchie RO. The true toughness of human cortical bone measured with realistically short cracks. Nat Mater 2008;7:672–7.
[20] Nalla RK, Kruzic JJ, Kinney JH, Ritchie RO. Mechanistic aspects of fracture and R-curve behavior in human cortical bone. Biomaterials 2005;26:217–31.
[21] Norman TL, Nivargikar SV, Burr DB. Resistance to crack growth in human cortical bone is greater in shear than in tension. J Biomech 1996;29:1023–31.
[22] Peterlik H, Roschger P, Klaushofer K, Fratzl P. From brittle to ductile fracture of bone. Nat Mater 2006;5:52–5.
[23] Vashishth D, Gibson GJ, Khoury JI, Schaffler MB, Kimura J, Fyhrie DP. Influence of nonenzymatic glycation on biomechanical properties of cortical bone. Bone 2001;28:195–201.
[24] Wang X, Bank RA, TeKoppele JM, Agrawal CM. The role of collagen in determining bone mechanical properties. J Orthop Res 2001;19:1021–6.

[25] Zimmermann EA, Schaible E, Bale H, Barth HD, Tang SY, Reichert P, et al. Age-related changes in the plasticity and toughness of human cortical bone at multiple length scales. Proc Natl Acad Sci USA 2011;108:14416–21.
[26] Zioupos P, Currey JD. Changes in the stiffness, strength, and toughness of human cortical bone with age. Bone 1998;22:57–66.
[27] Burr DB, Milgrom C, Fyhrie D, Forwood M, Nyska M, Finestone A, et al. In vivo measurement of human tibial strains during vigorous activity. Bone 1996;18:405–10.
[28] Lanyon LE, Hampson WGJ, Goodship AE, Shah JS. Bone deformation recorded invivo from strain gauges attached to human tibial shaft. Acta Orthop Scand 1975;46:256–68.
[29] Rubin CT, Lanyon LE. Limb mechanics as a function of speed and gait – a study of functional strains in the radius and tibia of horse and dog. J Exp Biol 1982;101:187–211.
[30] Robinovitch SN, Hayes WC, McMahon TA. Prediction of femoral impact forces in falls on the hip. J Biomech Eng 1991;113:366–74.
[31] Hansen U, Zioupos P, Simpson R, Currey JD, Hynd D. The effect of strain rate on the mechanical properties of human cortical bone. J Biomech Eng 2008;130:011011.
[32] Adharapurapu RR, Jiang F, Vecchio KS. Dynamic fracture of bovine bone. Mater Sci Eng C 2006;26:1325–32.
[33] Behiri JC, Bonfield W. Fracture-mechanics of bone – the effects of density, specimen thickness and crack velocity on longitudinal fracture. J Biomech 1984;17:25–34.
[34] Carter DR, Hayes WC. The compressive behavior of bone as a two-phase porous structure. J Bone Joint Surg Am 1977;59:954–62.
[35] Crowninshield RD, Pope MH. The response of compact bone in tension at various strain rates. Ann Biomed Eng 1974;2:217–25.
[36] Evans GP, Behiri JC, Vaughan LC, Bonfield W. The response of equine cortical bone to loading at strain rates experienced in vivo by the galloping horse. Equine Vet J 1992;24:125–8.
[37] Kirchner H. Ductility and brittleness of bone. Int J Fract 2006;139:509–16.
[38] Kulin RM, Jiang F, Vecchio KS. Loading rate effects on the R-curve behavior of cortical bone. Acta Biomater 2011;7:724–32.
[39] Kulin RM, Jiang F, Vecchio KS. Effects of age and loading rate on equine cortical bone failure. J Mech Behav Biomed 2011;4:57–75.
[40] McElhaney JH. Dynamic response of bone and muscle tissue. J Appl Physiol 1966;21:1231–6.
[41] Wright TM, Hayes WC. Tensile testing of bone over a wide range of strain rates: effects of strain rate, microstructure and density. Med Biol Eng 1976;14:671–80.
[42] Zioupos P, Hansen U, Currey JD. Microcracking damage and the fracture process in relation to strain rate in human cortical bone tensile failure. J Biomech 2008;41:2932–9.
[43] Gupta HS, Seto J, Wagermaier W, Zaslansky P, Boesecke P, Fratzl P. Cooperative deformation of mineral and collagen in bone at the nanoscale. Proc Natl Acad Sci USA 2006;103:17741–6.
[44] Hexemer A, Bras W, Glossinger J, Schaible E, Gann E, Kirian R, et al. A SAXS/WAXS/GISAXS beamline with multilayer monochromator. JPCS 2010;247:012007.
[45] Barth HD, Launey ME, MacDowell AA, Ager JW, Ritchie RO. On the effect of x-ray irradiation on the deformation and fracture behavior of human cortical bone. Bone 2010;46:1475–85.
[46] Ilavsky J. Nika: software for two-dimensional data reduction. J Appl Crystallogr 2012;45:324–8.
[47] Schindelin J, Arganda-Carreras I, Frise E, Kaynig V, Longair M, Pietzsch T, et al. Fiji: an open-source platform for biological-image analysis. Nat Methods 2012;9:676–82.
[48] E08 Committee. E1820-09 Standard Test Method for Measurement of Fracture Toughness. ASTM International; 2009.
[49] Koester KJ, Barth HD, Ritchie RO. Effect of aging on the transverse toughness of human cortical bone: evaluation by R-curves. J Mech Behav Biomed 2011;4:1504–13.
[50] Currey JD. The effects of strain rate, reconstruction and mineral content on some mechanical properties of bovine bone. J Biomech 1975;8:81–6.
[51] He MY, Hutchinson JW. Crack deflection at an interface between dissimilar elastic-materials. Int J Solids Struct 1989;25:1053–67.
[52] Imbeni V, Kruzic JJ, Marshall GW, Marshall SJ, Ritchie RO. The dentin–enamel junction and the fracture of human teeth. Nat Mater 2005;4:229–32.
[53] Chan KS, Nicolella DP. Micromechanical modeling of R-curve behaviors in human cortical bone. J Mech Behav Biomed 2012;16:136–52.
[54] Barth HD, Zimmermann EA, Schaible E, Tang SY, Alliston T, Ritchie RO. Characterization of the effects of x-ray irradiation on the hierarchical structure and mechanical properties of human cortical bone. Biomaterials 2011;32:8892–904.
[55] Busse B, Bale H, Zimmermann EA, Panganiban B, Barth HB, Carriero A, et al. Vitamin D deficiency induces early signs of aging in human bone, increasing the risk of fracture. Sci Transl Med 2013;5. 193ra188.
[56] Gupta HS, Krauss S, Kerschnitzki M, Karunaratne A, Dunlop JWC, Barber AH, et al. Intrafibrillar plasticity through mineral/collagen sliding is the dominant mechanism for the extreme toughness of antler bone. J Mech Behav Biomed 2013;28:366–82.
[57] Gautieri A, Vesentini S, Redaelli A, Buehler MJ. Viscoelastic properties of model segments of collagen molecules. Matrix Biol 2012;31:141–9.
[58] Zhang Z, Zhang Y-W, Gao H. On optimal hierarchy of load-bearing biological materials. Proc R Soc B 2011;278:519–25.
[59] Sasaki N, Shukunami N, Matsushima N, Izumi Y. Time-resolved x-ray diffraction from tendon collagen during creep using synchrotron radiation. J Biomech 1999;32:285–92.
[60] Hang F, Barber AH. Nano-mechanical properties of individual mineralized collagen fibrils from bone tissue. J R Soc Interface 2011;8:500–5.
[61] Tai K, Dao M, Suresh S, Palazoglu A, Ortiz C. Nanoscale heterogeneity promotes energy dissipation in bone. Nat Mater 2007;6:454–62.